Strong Anisotropic Order Parameters at All-Nitride Ferromagnet/Superconductor Interfaces

Qiao Jin[1†], Meng Yang[1,2†], Guozhu Song[3], Nan Zhao[3], Shengru Chen[1,2], Haitao Hong[1,2], Ting Cui[1,2], Dongke Rong[1,2], Qianying Wang[1,2], Yiyan Fan[1], Chen Ge[1,2,4], Can Wang[1,2,4], Jiachang Bi[5], Yanwei Cao[5], Liusuo Wu[3], Shanmin Wang[3], Kui-Juan Jin[1,2,4*], Zhi-Gang Cheng[1,4*], and Er-Jia Guo[1,2*]

[1]*Beijing National Laboratory for Condensed Matter Physics, and Institute of Physics, Chinese Academy of Sciences, Beijing 100190, China*
[2]*Department of Physics & Center of Materials Science and Optoelectronics Engineering, University of Chinese Academy of Sciences, Beijing 100049, China*
[3]*Department of Physics, Southern University of Science and Technology, Shenzhen 518055, China*
[4]*Songshan Lake Materials Laboratory, Dongguan 523808, China*
[5]*Ningbo Institute of Materials Technology & Engineering, Chinese Academy of Sciences, Ningbo 315201, China*

(Received 15 November 2023; accepted manuscript online 23 January 2024)

Proximity effects between superconductors and ferromagnets (SC/FM) hold paramount importance in comprehending the spin competition transpiring at their interfaces. This competition arises from the interplay between Cooper pairs and ferromagnetic exchange interactions. The proximity effects between transition metal nitrides (TMNs) are scarcely investigated due to the formidable challenges of fabricating high-quality SC/FM interfaces. We fabricated heterostructures comprising SC titanium nitride (TiN) and FM iron nitride (Fe_3N) with precise chemical compositions and atomically well-defined interfaces. The magnetoresistance of Fe_3N/TiN heterostructures shows a distinct magnetic anisotropy and strongly depends on the external perturbations. Moreover, the superconducting transition temperature T_C and critical field of TiN experience notable suppression when proximity to Fe_3N. We observe the intriguing competition of interfacial spin orientations near T_C (~ 1.25 K). These findings not only add a new materials system for investigating the interplay between superconductor and ferromagnets, but also potentially provide a building block for future research endeavors and applications in the realms of superconducting spintronic devices.

DOI: 10.1088/0256-307X/41/2/027402

Transition metal nitrides (TMNs) constitute a class of strongly correlated materials wherein nitrogen atoms are incorporated into the interstitial sites of the crystal lattices of parent metals.[1] These materials exhibit remarkable attributes such as exceptional corrosion resistance and hardness. Additionally, they encompass a spectrum of physical properties including ferroelectricity, superconductivity, and ferromagnetism.[2–6] TMNs are poised for devices under ambient conditions and emerge as promising candidates for functional layers in the realm of microelectronic devices. This encompasses applications such as nonvolatile memories, microwave devices, and electrochemical energy applications.[7–11] Within these novel applications, the superconducting quantum computing stands out as a highly significant domain of research within functional electronic devices. The interplay between a ferromagnet (FM) and a superconductor (SC) plays a pivotal role in performance of future devices.[12,13] As a ferromagnetic layer, the Cooper pairs within a superconducting film interact with spins, yielding novel and intricate interface effects within an FM/SC heterostructure. One noteworthy outcome is the proximity effect, giving rise to periodic oscillations in the superconducting order parameter of the ferromagnet, coupled with the injection of spin-triplet supercurrents into the ferromagnet. Recent research has culminated in the realization of a field-free Josephson diode within a van der Waals heterostructure,[14,15] demonstrating a significant advancement in the field.

Proximity effects have been extensively investigated across various functional materials, including metals, oxides, and chalcogenides.[16–20] In TMN superconductors, notable examples contain zirconium nitride,[21] hafnium nitride,[22] titanium nitride (TiN),[23] and vanadium nitride (VN).[24,25] Nonetheless, there exists a notable gap in the study of proximity effects within all-nitride ferromagnet/superconductor (FM/SC) interfaces. This scarcity of research can be attributed primarily to the intricate nature of preparing single-crystalline TMN thin films that possess high crystallinity and correct stoichiometry. These challenges hinder the establishment of well-defined interfaces as well. Recent years, our research group has achieved success in fabricating high-quality nitride single films and heterostructures using pulsed laser deposition (PLD) technique equipped with an atomic nitrogen plasma source. The highly active nitrogen atoms react with transition metals effectively so that the nitrogen vacancies can be largely compensated. With this technique, stoichiometric CrN films with variable thickness and orientation have

†These authors contributed equally to this work.
*Corresponding authors. Email: kjjin@iphy.ac.cn; zgcheng@iphy.ac.cn; ejguo@iphy.ac.cn
© 2024 Chinese Physical Society and IOP Publishing Ltd

been fabricated.[26–28] Their metal-to-insulator transition was observed and correlated to the evolution of band structure. Furthermore, a sizable exchange bias was observed in CrN/Fe_3N heterostructures and can be modulated by bending curvature.[29] Recently, we have observed a synergistic spin alignment at the Fe_3N/VN interface.[30] This alignment emerges due to the influence of the robustly ferromagnetic Fe_3N, which induces a magnetic moment within the superconducting VN. Similarly, TiN mirrors the characteristics of VN, as it represents a prototypical interstitial-nitride superconductor and is expected to have a similar magnetic proximity effect.

In this work, we fabricated high-quality TiN single films and Fe_3N/TiN heterostructures with atomically sharp interfaces. The superconducting transition temperature of TiN was suppressed apparently when proximity to the ferromagnetic Fe_3N. In addition, through electrical measurements, the ferromagnetic-to-superconducting transition was observed with magnetic field decreasing. This transition can be attributed to the competition between exchange interaction and spin orientation of Cooper pairs at interface, which occurs within a few nanometers. Our results not only present experimental foundations for all-nitride FM/SC interfaces, but also suggest the potential to manipulate the order parameters of ferromagnetism and superconductivity.

TiN has a cubic rocksalt structure, while ε-phase Fe_3N (ε-Fe_3N, abbreviated as Fe_3N hereafter) has a hexagonal structure at ambient conditions. As shown in Figs. 1(a) and 1(b), when viewed along the [111] direction, TiN consists of alternating atomic planes of Ti and N atoms with a hexagonal structure, which is similar to that of the (100) surface of Fe_3N. The atomic distance between two Ti atoms is 3.10 Å, as well as the atomic distance between two Fe atoms is 2.75 Å, which is close to the atomic distance between two Al atoms (2.77 Å) in sapphire (α-Al_2O_3, $R\bar{3}c$), as depicted in Fig. 1(c). When (111)-oriented TiN thin films grow on α-Al_2O_3 (0001) substrates, they suffer a large compressive strain up to −10.6%. We attribute such extraordinary phenomena to the high bulk moduli of TiN compared to conventional transition metal oxides. Moreover, the twining domains in TiN 111 films enhance their ability to sustain compressive strain.[27]

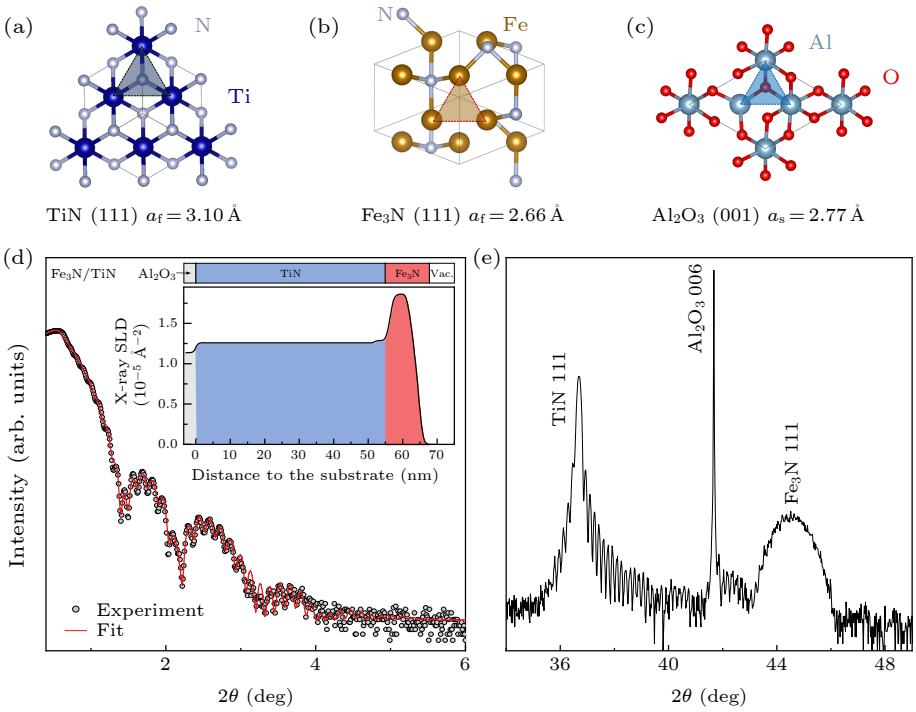

Fig. 1. Structural characterizations of Fe_3N/TiN heterostructures. (a)–(c) Planar views of crystal structures for (111)-TiN, (111)-Fe_3N, and (001)-Al_2O_3 planes, respectively. (d) XRR of Fe_3N/TiN heterostructures grown on Al_2O_3 substrates. The open symbols represent the experimental data, and the red line represents the best fit. Inset: x-ray scattering length density (SLD) depth profiles, indicating the chemical compositions of Fe_3N/TiN heterostructures. (e) The θ–2θ scan of Fe_3N/TiN heterostructures grown on Al_2O_3 substrates.

TiN thin films were synthesized on α-Al_2O_3 (0001) single-crystalline substrates via a homemade radio-frequency (RF) magnetron sputtering at a base pressure of 3×10^{-8} Torr. The growth conditions were meticulously optimized by varying the substrate temperature, gas components, RF power, and target-substrate distance.[31,32] The Fe_3N thin films were fabricated using self-designed PLD assisted by an atomic nitrogen plasma source. The XRR results in Fig. 1(d) exhibit clear thickness fringes, indicating atomically sharp and smooth interfaces within the bilayer. Analysis of the XRR results with the GenX software yielded the thickness-dependent x-ray SLD profile of the Fe_3N/TiN heterostructures [inset of Fig. 1(d)], revealing approximate layer thicknesses of 10 nm for Fe_3N

and 55 nm for TiN, respectively. The chemical roughness at the Fe_3N/TiN interfaces was estimated to be around 5 Å. The atomic density of TiN near the interface was found to slightly increase due to the structural deformation between TiN and the upper Fe_3N due to the large lattice mismatch of ∼14%. Notably, the surface density of the Fe_3N/TiN heterostructures was observed to be lower than that at the interface due to the oxidation of Fe ions. The topmost Fe_3N transformed into Fe_3O_4 upon exposure to air, yet we posit that this oxidized surface layer does not compromise the quality and exchange coupling at the Fe_3N/TiN interface. Long-range θ–2θ scans performed via synchrotron x-ray diffraction (sXRD) at beamline 1W1A of the Beijing Synchrotron Facility (BSRF) corroborated the epitaxial growth of the Fe_3N/TiN bilayer, as evidenced by single-orientation reflections from both layers and substrates. The XRD results shown in Fig. 1(e) illustrate that both Fe_3N and TiN layers are (111)-oriented. The discernible Laue fringes attest to the high crystallinity of the as-grown bilayers. Furthermore, the narrow rocking curves at TiN 111 and Fe_3N 111 reflections with a full width at half maximum of approximately 0.04° and 0.06°, respectively, were comparable to that of the Al_2O_3 substrate (approximately 0.02°). Overall, the structural characterizations of the Fe_3N/TiN heterostructures suggest that both layers were epitaxially grown, exhibiting uniform chemical composition.

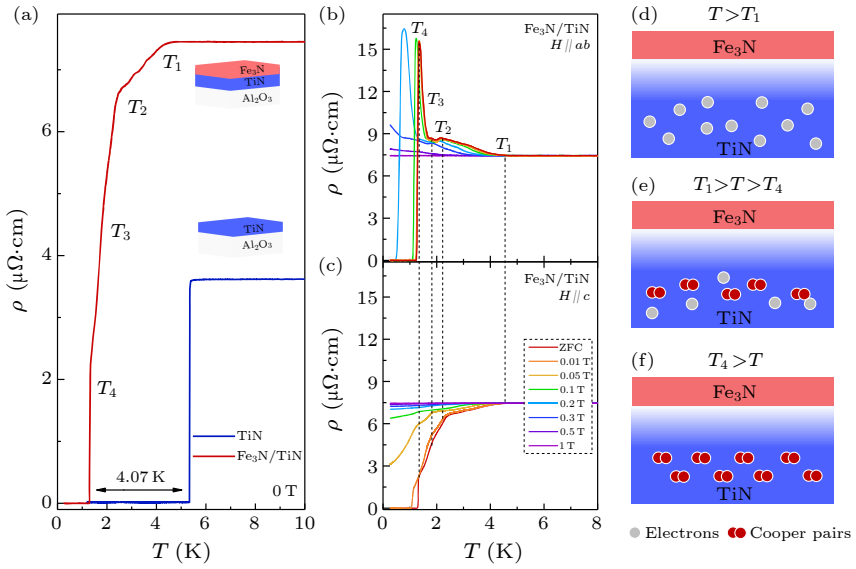

Fig. 2. Transport behavior of Fe_3N/TiN heterostructures. (a) Comparison of ρ–T curves between TiN single films and Fe_3N/TiN heterostructures at zero magnetic field. T_1 to T_4 were the resistivity transition points. T_C of TiN was suppressed by ∼4.07 K. Temperature-dependent resistivity of Fe_3N/TiN heterostructures when the various magnetic field was applied parallel to (b) the *ab*-plane and (c) the *c*-axis, respectively. (d)–(f) Schematic illustrations of the metal-insulator-superconductor transition at different temperature and field conditions.

Transport measurements on both TiN single films and Fe_3N/TiN heterostructures were conducted using the van der Pauw method with a wire-bonding technique. A standard lock-in technique was employed, operating at a frequency of 17 Hz and a current of 1 μA. The measurements were carried out within a physical properties measurement system equipped with a dilution refrigerator (Triton500; Oxford Instruments). As depicted in Fig. 2(a), the temperature-dependent resistivity (ρ–T) of both samples at zero field revealed metallic phases across all temperatures, transiting to superconducting states at lower temperatures. The onset of the superconducting transition temperature (T_C^{onset}) was identified as the temperature at which the resistivity commences decreasing for both samples. While the T_C^{onset} of Fe_3N/TiN heterostructures is comparable to that of the TiN single films, the T_C^{zero} of Fe_3N/TiN heterostructures decreases by approximately 4 K. Such behavior may originate from the suppression of superconducting order parameters by proximity to a ferromagnet. Additionally, the non-negligible magnetic impurity at the Fe_3N/TiN interfaces due to the chemical intermixing may also contribute to the suppressed superconductivity.[33–35] Hall measurements reveal that the majority charge carriers are electrons, with carrier densities of 8.36×10^{22} cm^{-3} for the TiN single films and 6.8×10^{22} cm^{-3} for Fe_3N/TiN heterostructures, as indicated in Table 1. The ρ–T curves of TiN single films exhibit a distinct sharp phase transition under both in-plane and out-of-plane magnetic fields (see Fig. S1 in the Supplementary Materials). Additionally, there is an observed low-temperature shift of T_C with an increase in the magnetic field. Notably, the superconductivity of TiN becomes entirely suppressed when $\mu_0 H$ exceeds 0.2 T.

The resistance–temperature (ρ–T) curves of TiN single films exhibit a distinct sharp phase transition under both in-plane and out-of-plane magnetic fields (refer to Fig. S1 in the Supplementary Materials). Additionally, there is an observed low-temperature shift of TC with an increase in the magnetic field. Notably, the superconductivity of TiN becomes entirely suppressed when the applied magnetic

field ($\mu_0 H$) exceeds 0.2 T

Figures 2(b) and 2(c) show the ρ–T curves of Fe_3N/TiN heterostructures under different magnetic fields when $H//ab$ and $H//c$, respectively. The dashed lines show the four resistivity drops of Fe_3N/TiN heterostructures in both in-plane and out-of-plane ρ–T curves, marked as T_1 to T_4, with decreasing temperature. We find that the Fe_3N/TiN heterostructures exhibits strong field dependent anisotropy. When the magnetic field increases along the c-plane, we note that the Fe_3N/TiN heterostructures maintain metallic phase but undergo multiple kinks at low temperatures. As the magnetic field increases along the ab-axis direction, we observe anomalous resistivity peaks at around T_C. The Fe_3N/TiN heterostructures exhibit a metal-insulator-superconductor transition with decreasing temperature. The amplitude of resistivity anomaly reaches $\sim 100\%$. This effect has been reported in low-dimensional thin films and 1D microstructures before.[36–40] Previously, different models were used to explain the nature of this resistivity anomalous peak, such as disorder and sample inhomogeneity, vortex dynamics and Josephson coupling in the layered systems, and competition between superconducting and insulating states in 2D systems. We interpret our observations in the framework of an empirical model induced by anisotropic disorder in TiN films when proximity to the ferromagnetic Fe_3N layers. When $T > T_1$, TiN is in the normal metallic state [Fig. 2(d)]. When $T_1 > T > T_4$ [Fig. 2(e)], the localized islands of Cooper pairs in TiN are formed, thus the number of free electrons reduces, resulting in a steep resistivity increase in the TiN films. When further reducing the temperature ($T_4 > T$) [Fig. 2(f)], the percolation through these localized islands, the TiN films turn into superconductor leading to zero resistance.

Moreover, we conducted measurements of the resistivities for both TiN single films and Fe_3N/TiN heterostructures as a function of magnetic field at various temperatures (see Fig. S2 in the Supplementary Materials, and Fig. 3). Figure 3(a) shows the magnetoresistance (MR) of TiN single films and Fe_3N/TiN heterostructures at 0.3 K with the magnetic field applied parallel to the ab-plane. The magnetic field was swept at a rate of 0.1 T/min from +5 T to −5 T (forward scans) and then at the same rate from −5 T to +5 T (reverse scans). Both TiN single films and Fe_3N/TiN heterostructures exhibit significant anisotropy in their magnetoresistance, as illustrated in Figs. 3(b) and 3(c), a characteristic trait of 2D superconductors. Notably, we observed that the resistivity anomaly induced by the magnetic field shifts from the out-of-plane to the in-plane direction upon the addition of a Fe_3N layer. Our hypothesis revolves around the magnetization of the interfacial TiN layer due to the inverse proximity effect from the ferromagnetic capping layer. This phenomenon leads to a substantial reduction in the thickness of the superconductive layer. Consequently, in Fe_3N/TiN heterostructures, the percolation through localized Cooper pair islands becomes more pronounced along the in-plane direction. We determined the upper critical magnetic fields (H_{C2}) where the resistivity reduces to zero for both TiN single films and Fe_3N/TiN heterostructures. Specifically, for TiN single films, H_{C2} ($H//ab$) was found to be approximately 1.04 T, which is larger than H_{C2} ($H//c$) at approximately 0.33 T at 0.3 K. Notably, we observed a reduction of approximately 60% in the H_{C2} for Fe_3N/TiN heterostructures when TiN was capped with a strong ferromagnet. Consequently, the presence of ferromagnetism across the interfaces significantly suppresses the superconductivity.

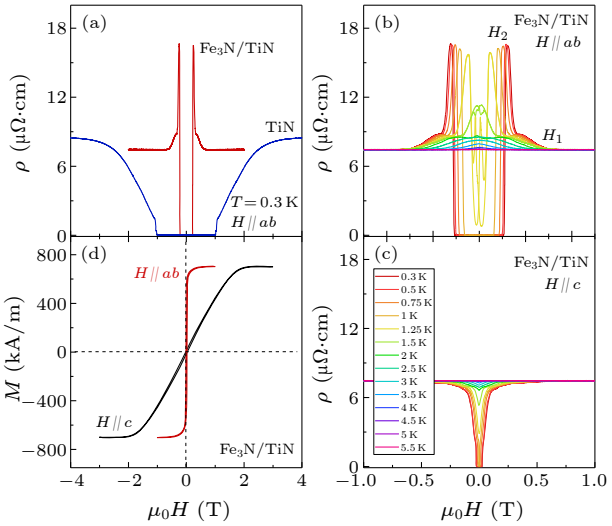

Fig. 3. Field-dependent resistivity and magnetization of Fe_3N/TiN heterostructures. (a) Comparison of in-plane field-dependent resistivity between TiN single films and Fe_3N/TiN heterostructures at 0.3 K. Magnetic-field dependent resistivity of Fe_3N/TiN heterostructures at various temperatures when the magnetic field was applied parallel to (b) the ab-plane and (c) the c-axis, respectively. (d) M–H hysteresis loops of Fe_3N/TiN heterostructures at 10 K for both in-plane and out-of-plane magnetic fields.

To comprehensively analyze the field-induced suppression of superconductivity in TiN, we plot the temperature-dependent H_{C2} for both TiN single films and Fe_3N/TiN heterostructures, as depicted in Fig. 4(a). We observe a pronounced anisotropy of H_{C2} under varying field polarities, with notable reductions by factors of five and ten for $H//ab$ and $H//c$, respectively. The experimental data were fitted using a single-band Werthamer–Helfand–Hohenberg (WHH) model:[41,42]

$$\ln t + \psi\left(\frac{1}{2} + h\right) - \psi\left(\frac{1}{2}\right) = 0, \tag{1}$$

where $t = T/T_C$ is reduced temperature, $h = \frac{\mu_0 H_{C2} \hbar D}{2\varphi_0 k_B T}$, $\hbar$ is Planck's constant, k_B is Boltzmann's constant, D is the diffusion coefficient, φ_0 is the flux quantum, and ψ is the digamma function. Furthermore, we calculated the Fermi vector (v_f), coherence length (L_C), and mean free path (λ) using the following equations for both samples:

$$v_f = \frac{\hbar k_f}{m} = \frac{\hbar}{m}(3\pi^2 n)^{1/3}, \tag{2}$$

$$\lambda \approx 0.18 \frac{\hbar k_f}{k_B T_C}, \tag{3}$$

$$L_C = v_f \tau = v_f m/(ne^2\rho), \tag{4}$$

where m is the electron mass, n is the electron density; λ is one order of magnitude larger than L_C, suggesting that these values are in the dirty limit for both films. The results are listed in Table 1. After capping a ferromagnetic

Fe_3N layer, L_C was reduced by a factor of four whereas the λ and v_f remained nearly constant, indicating a strong competition of superconductivity and ferromagnetic across Fe_3N/TiN interfaces.

Table 1. Summary of the parameters for the TiN superconducting single films and Fe_3N/TiN heterostructures, including superconducting transition temperature (T_C), upper critical field (H_{C2}) at zero temperature fitting by WHH model, carrier density (n), Fermi vector (v_f), coherence length (L_C), and mean free path (λ). The electronic parameters, such as resistivities, carrier densities, and mobilities, of single layer and bilayers were extracted from the transport measurements conducted in the normal state (at 10 K). Estimated errors are listed in parentheses.

	TiN	Fe_3N/TiN
T_C (K)	5.35(5)	1.28(3)
H_{C2} ($H//ab$) (T)	1.04(6)	0.23(4)
H_{C2} ($H//c$) (T)	0.33(5)	0.03(2)
n (10^{22} cm^{-3})	8.36(3)	6.80(2)
v_f (10^6 m/s)	1.56(4)	1.46(2)
L_C (nm)	401(3)	1568(3)
λ (nm)	11.85(2)	10.21(5)

Furthermore, the presence of the inverse proximity effect at the interfaces of ferromagnet/superconductor often results in the formation of a magnetic interfacial layer within the superconductor. We conducted measurements of both in-plane and out-of-plane magnetizations on Fe_3N/TiN heterostructures versus the magnetic field, as shown in Fig. 3(d). The magnetic easy axis aligns along the in-plane direction, exhibiting a coercive field of approximately 120 Oe. Furthermore, the saturation magnetization of Fe_3N/TiN heterostructures reaches approximately 700 kA/m. Currently, it remains unclear whether there is an induced magnetic moment in the interfacial TiN layer. Future experimental confirmation through polarized neutron reflectometry measurements will be necessary for clarification.[43,44] We conducted ac magnetization measurements on Fe_3N/TiN heterostructures below 1 K at Southern University of Science and Technology (SUSTech) using a dilution refrigerator system (see Fig. S3 in the Supplementary Materials). At temperatures where resistivity exhibits an upturn, distinct diamagnetic signals emerged, indicating the occurrence of the insulator-superconducting transition. In addition, MR measurements were conducted slightly above or below T_C under different magnetic fields, as shown in Figs. 4(b) and 4(c) for in-plane and out-of-plane magnetic fields, respectively. At a temperature of 1 K, the resistivity of Fe_3N/TiN heterostructures rapidly drops to zero as the in-plane magnetic field decreases to approximately 0.13 T. However, at a temperature of 1.25 K, we did not observe a complete emergence of zero resistivity. Instead, we noted a suppression of the anomalous resistivity peaks originating from the superconducting TiN. Additionally, Fe_3N/TiN heterostructures exhibited symmetric MR peaks at small magnetic fields, attributed to the coercive fields of the ferromagnetic layers. As the temperature exceeded 1.25 K, the anomalous resistivity peaks disappeared, and the MR of Fe_3N/TiN heterostructures exhibited typical ferromagnetic responses, possibly arising from the Fe_3N or magnetic interfacial layers.

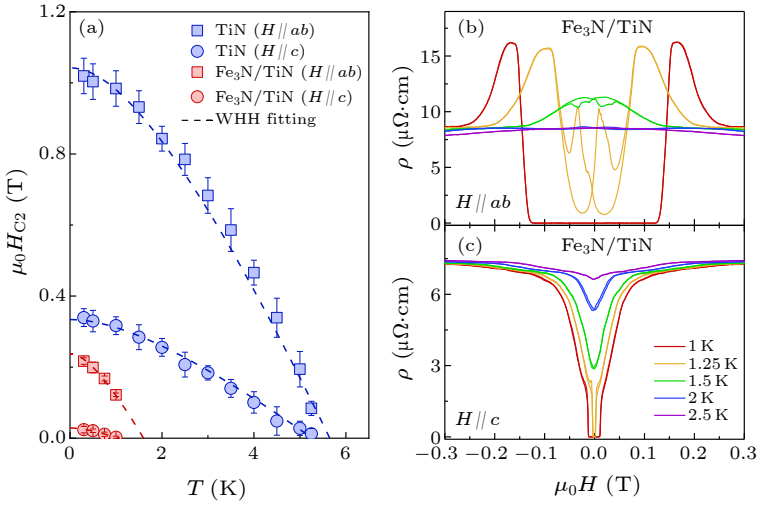

Fig. 4. Suppression of superconducting order parameters by a strong ferromagnet. (a) Temperature dependence of upper critical field (H_{C2}) for TiN single films and Fe_3N/TiN heterostructures. The square and circle symbols represent H_{C2} when the magnetic field was applied parallel to the ab-plane and the c-axis, respectively. The dashed lines are fitting curves based on the Werthamer–Helfand–Hohenberg (WHH) model. The fitting parameters are summarized in Table 1. [(b), (c)] Zoom-in view of field-dependent resistivity of Fe_3N/TiN heterostructures across T_C when $H//ab$ and $H//c$, respectively.

In summary, our findings demonstrate the inhibition of superconductivity in all-nitride heterostructures through the proximity effect between high-quality ferromagnetic Fe_3N and superconductive TiN. Expanding on our previous research, we aim to clarify the competitive dynamics occurring at the interface between ferromagnetic and superconducting materials based on transition metal nitrides. This interface presents a new avenue for exploring superconducting order parameters. Specifically, the recent discovery of parallel spin alignments across nitride inter-

faces holds the potential to decrease electron scattering. This effect offers additional components for developing superconducting quantum devices, such as Josephson supercurrent diodes.

Acknowledgements. We thank Professor Kun Jiang (IOP-CAS), Professor Guoqiang Yu (IOP-CAS), Professor Enke Liu (IOP-CAS), and Professor Zhiqi Liu (BUAA) for fruitful discussions. This work was supported by the National Key Research and Development Program of China (Grant Nos. 2020YFA0309100 and 2019YFA0308500), the National Natural Science Foundation of China (Grant Nos. U22A20263, 52250308, and 11974390), the CAS Project for Young Scientists in Basic Research (Grant No. YSBR-084) (E.J.G.), Special Research Assistant (Q.J.), the Strategic Priority Research Program (B) of the Chinese Academy of Sciences (Grant No. XDB33030200) (K.J.), the China Postdoctoral Science Foundation (Grant No. 2022M723353), and the Guangdong-Hong Kong-Macao Joint Laboratory for Neutron Scattering Science and Technology (Grant No. HTCSNS-DG-CD-0080/2021). PNR experiments were conducted at the Beamline MR of Chinese Spallation Neutron Source, CAS. The synchrotron-based XRD measurements were performed at the beamline 1W1A of the Beijing Synchrotron Radiation Facility (BSRF) via user proposals.

References

[1] Bhattacharyya S 2015 *J. Phys. Chem. C* **119** 1601
[2] Mei A B, Hellman O, Wireklint N, Schlepütz C M, Sangiovanni D G, Alling B, Rockett A, Hultman L, Petrov I, and Greene J E 2015 *Phys. Rev. B* **91** 054101
[3] Coey J M D and Smith P A I 1999 *J. Magn. Magn. Mater.* **200** 405
[4] Talley K R, Perkins C L, Brennecka G L, and Zakutayev A 2021 *Science* **374** 1488
[5] Akiyama M, Kamohara T, Kano K, Takeuchi Y, and Kawahara N 2009 *Adv. Mater.* **21** 593
[6] Gu Y, Jiang K, Wu X, and Hu J 2022 *Chin. Phys. Lett.* **39** 097401
[7] Bai Y, Wang Z, Lei N, Muhammad W, Xiang L, Li Q, Lai H, Zhu Y, Wang W, Guo H, Yin L, Wu R, and Shen J 2022 *Chin. Phys. Lett.* **39** 108501
[8] Ningthoujam R S and Gajbhiye N S 2015 *Prog. Mater. Sci.* **70** 50
[9] Wang H, Li J, Li K, Lin Y, Chen J, Gao L, Xiao X, and Lee J M 2021 *Chem. Soc. Rev.* **50** 1354
[10] Kim K H, Oh S, Fiagbenu M M A, Zheng J, Musavigharavi P, Kumar P, Trainor N, Aljarb A, Wan Y, Katti K, Song S, Kim G, Tang Z, Fu J H, Hakami M, Tung V, Redwing J M, Stach E A, Olsson III R H, and Jariwala D 2023 *Nat. Nanotechnol.* **18** 1044
[11] Kim K H, Karpov I, Olsson III R H, and Jariwala D 2023 *Nat. Nanotechnol.* **18** 422
[12] Ando F, Miyasaka Y, Li T, Ishizuka J, Arakawa T, Shiota Y, Yanase Y, and Ono T 2020 *Nature* **584** 373
[13] Hou Y S, Nichele F, Chi H, Lodesani A, Wu Y, Ritter M F, Haxell D Z, Davydova M, Ilić S, Glezakou-Elbert O, Varambally A, Bergeret F S, Kamra A, Lee P A, and Moodera J S 2023 *Phys. Rev. Lett.* **131** 027001
[14] Jeon K R, Kim J K, Yoon J, Jeon J C, Han H, Kontos T, and Parkin S S P 2022 *Nat. Mater.* **21** 1008
[15] Jeon K R, Hazra B K, Kim J K, Jeon J C, Han H, Meyerheim H L, Cottet A, and Parkin S S P 2023 *Nat. Nanotechnol.* **18** 747
[16] Mercaldo L V, Attanasio C, Coccorese C, Prischepa S L, and Salvato M 1996 *Phys. Rev. B* **53** 14040
[17] Mühge T, Garif'yanov N N, Goryunov Y V, Khaliullin G G, Tagirov L R, Garifullin I A, and Zabel H 1996 *Phys. Rev. Lett.* **77** 1857
[18] Deen P P, Yokaichiya F, de Santis A, Wildes A R, and Cucolo A M 2006 *Phys. Rev. B* **74** 224414
[19] Giblin S R, Taylor J W, Duffy J A, Butchers M W, Utfeld C, Dugdale S B, Visani C, and Santamaria J 2012 *Phys. Rev. Lett.* **109** 137005
[20] Satapathy D K, Uribe-Laverde M A, Marozau I, Malik V K, Das S, Wagner T, Marcelot C, Stahn J, Bruck S, Ruhm A, Macke S, Tietze T, Goering E, Frañó A, Kim J H, Wu M, Benckiser E, Keimer B, Devishvili A, Toperverg B P, Merz M, Schuppler S, and Bernhard C 2012 *Phys. Rev. Lett.* **108** 197201
[21] Choudhary K and Garrity K 2022 *npj Comput. Mater.* **8** 244
[22] Kroll P 2003 *Phys. Rev. Lett.* **90** 125501
[23] Kardakova A, Finkel M, Morozov D, Kovalyuk V, An P, Dunscombe C, Tarkhov M, Klapwijk M T, and Goltsman G 2013 *Appl. Phys. Lett.* **103** 252602
[24] Zou Y T, Jin Q, Wang Y X, Jiang K, Wang S M, Guo E J, and Cheng Z G 2022 *Phys. Rev. B* **105** 224516
[25] Ajami F I and Maccrone R K 1975 *J. Phys. Chem. Soilds* **36** 7
[26] Jin Q, Cheng H, Wang Z, Zhang Q, Lin S, Roldan M A, Zhao J L, Wang J O, Chen S, He M, Ge C, Wang C, Lu H B, Guo H Z, Gu L, Tong X, Zhu T, Wang S, Jin K J, and Guo E J 2021 *Adv. Mater.* **33** 2005920
[27] Jin Q, Wang Z, Zhang Q, Zhao J L, Cheng H, Lin S, Chen S, Guo H Z, He M, Ge C, Wang C, Wang J O, Gu L, Wang S, Jin K J, and Guo E J 2021 *Phys. Rev. Mater.* **5** 023604
[28] Jin Q, Zhao J L, Roldan M A, Qi W H, Lin S, Chen S, Hong H T, Fan Y Y, Rong D K, Guo H Z, Ge C, Wang C, Wang J O, Jin K J, and Guo E J 2022 *Appl. Phys. Lett.* **120** 073103
[29] Jin Q, Zhang Q H, Bai H, Huon A, Charlton T, Chen S R, Lin S, Hong H T, Cui T, Wang C, Guo H Z, Gu L, Zhu T, Fitzsimmons M R, Wang S M, and Guo E J 2023 *Adv. Mater.* **35** e2208221
[30] Jin Q, Zhang Q H, Bai H, Zou Y T, Ga Y L, Chen S R, Hong H T, Cui T, Rong D K, Wang J O, Wang C, Cao Y W, Gu L, Wang S M, Jiang K, Cheng Z G, Zhu T, Jin K J, and Guo E J 2023 arXiv:2304.05234
[31] Zhang R Y, Li X Y, Meng F Q, Bi J C, Zhang S D, Peng S Q, Sun J, Wang X M, Wu L, Duan J X, Cao H T, Zhang Q H, Huang L H, and Cao Y W 2021 *ACS Appl. Mater. Inter.* **13** 60182
[32] Zhang R Y, Ma Q Y, Liu H, Sun T Y, Bi J, Song Y, Peng S, Liang L, Gao J H, Huang L F, and Cao Y W 2021 *ACS Photon.* **8** 847
[33] Yazdani A, Jones B A, Crommie M F, and Eigler D M 1997 *Science* **275** 1767
[34] Smith R A and Ambegaokar V 2000 *Phys. Rev. B* **62** 5913
[35] Katano S, Shibata K, and Matsubara Y 2017 *Phys. Rev. B* **95** 144502
[36] Santhanam P, Chi C C, Wind S J, and Bucchignano J J 1991 *Phys. Rev. Lett.* **66** 2254
[37] Park M and Parpia J M 1997 *Phys. Rev. B* **55** 9067
[38] Wang H, Rosaria M M, and Liu Y 2007 *Phys. Rev. B* **75** 064509
[39] Zhang G F, Zeleznik M, May P W, and Moshchalkov V V 2013 *Phys. Rev. Lett.* **110** 077001
[40] Zhang G F, Samuely T, Kačmarčík J, Ekimov E A, Li J, Vanacken J, Szabó P, Huang J, Cerbu D, and Moshchalkov V V 2016 *Phys. Rev. Appl.* **6** 064011
[41] Werthamer N R, Helfand E, and Hohenberg P C 1966 *Phys. Rev.* **147** 295
[42] Tao Q, Shen J Q, Li L J, Lin X, Luo Y K, and Xu Z A 2009 *Chin. Phys. Lett.* **26** 097401
[43] Guo E J, Desautels R, Lee D, Roldan M A, Liao Z L, Charlton T, Ambaye H, Molaison J, Boehler R, Keavney D, Herklotz A, Ward T Z, and Fitzsimmons M R 2019 *Phys. Rev. Lett.* **122** 187202
[44] Guo E J and Zhu T 2019 *Physics* **48** 708 (in Chinese)